Layer-by-Layer Hydrogen-Bonded Antioxidant Films of Linear Synthetic Polyphenols

Raman Hlushko¹, John F. Ankner², and Svetlana Sukhishvili¹*

¹Department of Materials Science and Engineering, Texas A&M University

College Station, Texas 77843, USA

²Spallation Neutron Source, Oak Ridge National Laboratory, Oak Ridge, Tennessee 37831, USA

Abstract

We report on the role of the chemical structure of polyphenol pendant groups in linear antioxidant polymers on their assembly and chain intermixing within layer-by-layer (LbL) films, as well as on the antioxidant performance of the interfacial assemblies. When assembled with poly(ethylene oxide) (PEO) within hydrogen-bonded films, the antioxidant polymers – poly(3,4dihydroxybenzyl methacrylamide) (P2HMA) and poly(3,4,5-trihydroxybenzyl methacrylamide) (P3HMA) – which contain catechol- and gallol-like moieties, respectively, generated films with drastically different structure and functionality. Specifically, while catechol-based P2HMA deposited within LbL films linearly with a low increment of mass increase per step, growth of P3HMA/PEO films was strongly exponential. Dramatic differences in chain intermixing and layering in these films are revealed by the application of neutron reflectometry using deuterated PEO, dPEO, to create marker layers. Differences in film structure strongly affected film antioxidant performance, as demonstrated by radical scavenging assay. While assembled P3HMA was fully available for scavenging 2,2'-azino-bis(3-ethylbenzothiazoline-6-sulfonic acid) (ABTS⁺) radical cations, in assembled P2HMA radical scavenging was restricted to the top ~35 nm of the LbL film, highlighting the effect of the LbL film structure on antioxidant performance.

Introduction

Antioxidants can enhance the performance of polymers used in food packaging¹⁻⁴ or biomedical applications⁵ by reducing oxidative damage caused by reactive oxygen species. The most common approach of blending low molecular weight antioxidants into a polymer matrix^{1-4,6-8} is often associated, however, with leaching of antioxidants.⁹ To prevent leaching, antioxidant groups have been introduced into polymeric materials either via covalent modification of already synthesized polymers^{5,10-13} or via direct polymerization of antioxidant-bearing monomers.^{14,15} The latter approach allows for greater control of the distribution of antioxidant species along the polymer chain. Using this approach, antioxidant-bearing materials were used in the preparation of free-standing or substrate-deposited films using solution-casting.³

An alternative way to introduce antioxidant species into a surface coating is *via* layer-by-layer (LbL) assembly. The LbL deposition technique is a powerful means of creating nanoscopic coatings from a diverse set of components. ^{16,17} The most appealing features of the technique are the control it affords of film composition, structure, and thickness and its enabling the application of ultrathin coatings to arbitrarily shaped substrates. The degree to which the LbL technique can provide such control is strongly dependent on the strength of interpolymer binding within the films. While strong polymer-polymer pairing usually results in kinetically trapped conformations of sequentially adsorbed chains and preserves film layering, weak binding enables chain mobility, resulting in polymer intermixing. ¹⁸⁻²¹ The assembly of LbL films is generally supported by electrostatic pairing ^{16,17} and/or hydrogen bonding, ²²⁻²⁷ with both electrostatically associated and hydrogen bonded films able to be assembled linearly (a constant amount of material deposited per immersion step) or exponentially (an increasing amount of material deposited per immersion step). Because of the weak binding between polymer units within exponential films, these assemblies

can exhibit high swelling ratios, are highly diffusive, self-healing, ^{28,29} and in extreme cases can even exhibit swelling behavior characteristic of densely physically crosslinked, surface-attached gels. ³⁰ The polymer units which do not directly participate in electrostatic or hydrogen bonding polymer-polymer pairing remain available for supporting film functionality. In the case of electrostatic assemblies, these polymer units have been utilized, for example, for the capture of metal or organic ions. ³¹⁻³³ For hydrogen-bonded LbL assemblies, however, such structure-functionality correlations remain unexplored.

Our group has pioneered the deposition of hydrogen-bonded films composed of a small polyphenol molecule, tannic acid (TA), with neutral polymeric hydrogen-bond acceptors. 34,35 The low value of the TA ionization constant (p K_a 8.5) 34 enabled the creation of hydrogen-bonded assemblies stable at neutral to slightly basic pH 34 and thus the exploitation of the antioxidant, anti-inflammatory, and immuno-modulating properties of TA in biological environments. 36,37 In addition to TA, other small polyphenol molecules were reported as components of LbL films. $^{38-40}$ However, small molecules lack the connectivity of functional repeat units and thus are unable to supply an excess of unbound functional groups within LbL assemblies.

Here, we focus on hydrogen-bonded coatings created by LbL assembly of synthetic linear polyphenols (*IPPh*), recently synthesized in our group, ^{14,41} containing catechol or gallol functionalities. In our previous work, we demonstrated antioxidant activity of these polymers in solution. ¹⁴ In this work we focus on assembly of these polymers at surfaces and correlate the mechanism of film growth and layering with the antioxidant activity of these assemblies. The *IPPh* polymers, specifically those with gallol functional groups, can be viewed as synthetic analogs of tannic acid. Unlike TA, however, these polymers are flexible and capable of multisite binding with hydrogen-bonding partners, leaving some segments unbound to polymer partners. We aim to

explore how the chemistry of polyphenol moieties affects polymer-polymer binding, chain intermixing and film structure, as well as the availability of polyphenol segments for radical scavenging. We believe that this work significantly expands the arsenal of adhesive and antioxidant films and coatings based on phenolic functionality. 42,43

Materials

Polyethylene oxide (PEO) with M_n 100 kg/mol, branched polyethylene imine (BPEI) with M_n 60 kg/mol, 2,2′-azino-bis(3-ethylbenzothiazoline-6-sulfonic acid) (ABTS) diammonium salt, ethanol, sodium hydroxide, hydrochloric acid, sodium hydrogen phosphate, and potassium persulfate were purchased from Sigma-Aldrich and used as received. Deuterated poly(ethylene oxide-d4) (dPEO) with M_n 93.0 kg/mol and polydispersity index (PDI) 1.07 was purchased from Polymer Source Inc. Linear synthetic polyphenols (IPPh), poly(3,4-dihydroxybenzyl methacrylamide) (P2HMA, M_n 35.9 kg/mol, PDI 1.20) and poly(3,4,5-trihydroxybenzyl methacrylamide) (P3HMA, M_n 43.4 kg/mol, PDI 1.45), were synthesized and characterized as described in our previous work. ¹⁴ Koptec 200 proof ethanol, 99.5% (Millipore Sigma) and Milli-Q water with resistivity of 18 M

Film Deposition

Silicon substrates (<111>) used in neutron reflectivity experiments, as well as 0.5-mm thick undoped silicon wafers, both obtained from the Institute of Electronic Materials Technology, Poland, were cleaned as described elsewhere. ⁴⁴ Prior to film deposition, silicon substrates and/or wafers were primed with a robust monolayer of BPEI adsorbed from 0.2 mg/mL solution at pH 9 (where BPEI is weakly charged) for 20 min as described in our previous work⁴⁵ to eliminate the effect of different adhesiveness of *I*PPh polymers to silicon substrates, as well as to prevent delamination of the films from the substrates in solutions at high pH values. The LbL films were

then constructed from 0.2 mg/mL polymer solutions in ethanol or water for *IPPh* or PEO, respectively, because of the selective solubility of *IPPh* and PEO in these solvents. The substrates were immersed in the deposition solutions for 5 minutes per deposition step, rinsed twice in solvent, and dried in a gentle flow of nitrogen gas. Films thicker than 20 bilayers were deposited using a Riegler & Kirstein GmbH DR-3 table top dipping robot.

Spectroscopic Ellipsometry

Refractive indices and thicknesses of LbL films deposited on a silicon wafer were determined using a variable angle spectroscopic ellipsometer (M-2000, J.A. Woollam Co., Inc.) equipped with a temperature-controlled liquid cell. Dry measurements were performed at four incidence angles: 45, 55, 65, and 75°. A single incident angle of 75° was used in liquid-cell measurements due to cell geometry. The thicknesses of the native oxide layers on the silicon wafers were measured prior to depositing the LbL films.

The data for dry LbL films were fitted using a three-layer model. The first two layers were the silicon substrate and the oxide layer. The third layer was characterized as a Cauchy material of thickness d. The wavelength dependence of the refractive index was modeled by $n(\lambda) = A + B/\lambda^2 + C/\lambda^4$, where λ is wavelength and A, B, and C are fitted coefficients. For the swollen films, a four-layer model was used, wherein the solvent was considered as the fourth layer, characterized as a semi-infinite transparent Cauchy medium. The dependence of refractive index on wavelength was determined prior to each measurement using a bare silicon wafer installed in the liquid cell. The four variables A, B, C, and thickness d were fitted simultaneously.

Attenuated Total Reflection Fourier Transform Infrared (ATR-FTIR) Spectroscopy

ATR-FTIR spectra were collected using a Bruker Tensor II spectrometer equipped with a mercury cadmium telluride (MCT) detector and an ATR diamond crystal. The spectra were recorded by accumulating 96 scans within a spectral range of 900–4000 cm⁻¹ at a resolution of 2 cm⁻¹.

To assess the composition of the polyphenol films, *IPPh/PEO* films of~ 200 nm dry thickness deposited on undoped Si wafers were exposed to either *IPPh* or PEO 0.2 mg/mL solutions in ethanol for 5 minutes, followed by two cycles of solvent rinsing, and finally dried in a flow of nitrogen gas. FTIR spectra were collected after each deposited polymer layer.

Atomic Force Microscopy (AFM)

AFM studies were performed using a Bruker Dimension Icon AFM instrument in tapping mode using a MikroMasch HQ:NSC35/Cr-Au BS 150 kHz cantilever with a 5.4 N/m force constant. The average film roughness was measured over three imaged areas.

Nanoindentation

Mechanical properties of the films were studied using Hysitron TI 950 Triboindenter equipped with a diamond Berkovich tip with a radius of 150 nm. Indentation was performed in the load-controlled mode, where the load was increased at a constant rate for a 10 s up to a finite value, kept constant for 5 s and brought back to zero in 2 s. The applied load was set as 50 μ N for the 0.6 μ m films and 150 μ N for thicker films. The tip displacement was less than 10% of the total film thickness for all film. The Young's modulus of the films was calculated using the equation

$$\frac{1}{E_{eff}} = \frac{1 - v^2}{E} + \frac{1 - v_i^2}{E_i}$$

where E_{eff} is the measured effective elastic modulus, E and v are the Young's modulus and Poisson ratio of the film, E_i and v_i are Young's modulus and Poisson ratio of the diamond indenter, equal to 1141 GPa and 0.07, respectively. ⁴⁷ The Poisson ratio of the dry hydrogen-bonded films was set

at 0.33, and a value of 0.5 was used for wet measurements, a value which was previously used for LbL films. 48

Neutron Reflectometry

Neutron reflectometry measurements were performed at the Spallation Neutron Source Liquids Reflectometer (SNS-LR) at the Oak Ridge National Laboratory (ORNL). The reflectivity data were collected using a sequence of 3.4-Å-wide continuous wavelength bands (selected from 2.55 Å < λ < 16.70 Å) and incident angles (ranging over $0.6^{\circ} < \theta < 2.34^{\circ}$). The momentum transfer, $Q = (4\pi \sin \theta/\lambda)$, was varied over a range of 0.008 Å⁻¹ < Q < 0.20 Å⁻¹. Reflectivity curves were assembled by combining seven different wavelength and angle data sets together, maintaining a constant relative instrumental resolution of $\delta Q/Q = 0.023$ by varying the incident-beam apertures.

Neutron scattering densities within hydrogenated and deuterated blocks were averaged, each block exhibiting its characteristic thickness, scattering density, and interlayer roughness. Those characteristic parameters were adjusted until the reflectivity curve was best fitted (minimized χ^2).

Antioxidant Activity Studies

The antioxidant activity of *IPPh/PEO* coatings was studied using a radical scavenging assay employing aqueous solutions of ABTS⁺⁺ radical cations. The stock solution of ABTS⁺⁺ was prepared by mixing 10 mL of 7 mM ABTS and 10 mL of 2.45 mM potassium persulfate aqueous solutions. The stock solution was incubated in the dark at ambient temperature for 24 hours to complete the formation of ABTS⁺⁺ radical cations, and then diluted with water until the absorbance decreased to 1.0-2.0 absorbance units as measured at 732 nm using a 2600 UV-Vis Shimadzu spectrophotometer. The diluted solutions were purged with nitrogen gas for one hour and then immediately used for the antiradical assay. The antiradical efficiency of *IPPh/PEO* films was

monitored as a decrease in absorbances of diluted ABTS⁺⁺ solutions at 732 nm. Experiments were performed with films deposited on 0.5-0.8 cm² Si chips. To perform the radical scavenging assay, the substrates with deposited IPPh/PEO films as well as control bare Si wafers were placed in plastic cuvettes filled with 0.04 mM (in case of P3HMA/PEO films) or 0.06 mM (in case of P2HMA/PEO films) ABTS⁺⁺ solutions and sealed. At a sequence of times after exposure, the solutions were carefully shaken and the absorbance at 732 nm was recorded. The decrease in absorbance was converted to concentration of reacted ABTS⁺⁺ as $(A_0 - A)/\varepsilon$, where A_0 and A are the absorbances of the control ABTS⁺⁺ solutions and ABTS⁺⁺ solutions exposed to antioxidant films, respectively, and ε is the extinction coefficient of ABTS⁺⁺ solutions at 732 nm (ε = 25400 M⁻¹cm⁻¹).⁴⁹ Data for the reacted ABTS⁺⁺ were normalized to a 1 cm² film area. The antioxidant activity of IPPhs in solution was determined similarly from the decrease in the absorbance of 3.0 mL 0.075 mM ABTS⁺⁺ aqueous solution after addition of 100 μ L of 0.5 mg/mL polymer in ethanol.

RESULTS AND DISCUSSION

Fig. 1A shows the chemical structures of the two synthetic linear polyphenols (*IPPh*) used in this work. These polymers, poly(3,4-dihydroxybenzyl methacrylamide) (P2HMA) and poly(3,4,5-trihydroxybenzyl methacrylamide) (P3HMA), containing catechol and gallol pendant groups, respectively, were previously synthesized by our group using RAFT polymerization. ¹⁴ P2HMA and P3HMA had number-average molecular weights of 35.9 kg/mol and 43.4 kg/mol, and degrees of polymerization of 170 and 200, respectively (Fig. 1A). In previous work we showed that the structure of the polyphenol rings had a weak effect on intrinsic *IPPh* antioxidant activity but strongly affected the capability of these polymers to adsorb within a monolayer on a solid substrate.

Specifically, P3HMA, containing gallol-like pendant groups, had a higher propensity than P2HMA to adsorb to surfaces.¹⁴ This work aims to explore the capability of *IPPhs* of different chemical structure to assemble at surfaces within multilayers rather than monolayers. To that end, *IPPh* polymers have been assembled within functional LbL coatings with polyethylene oxide, which is used as a hydrogen-bonding partner.

Figure 1B shows the increase in dry film thickness during LbL film deposition measured by ellipsometry. Assembly occurs as a result of hydrogen bonding between hydroxyl groups in polyphenol units and PEO units. Films formed by PEO and IPPh with catechol functionality (P2HMA) grew linearly, with a 3.3-nm dry thickness increase per bilayer. In contrast, the P3HMA/PEO layers exhibited a dramatically different growth mode, forming much thicker films of exponentially increasing thickness per deposition step. The exponential growth of P3HMA/PEO films was somewhat counterintuitive since such growth is usually a characteristic of weakly associated polymers. 50,51 As a polyphenol with three hydroxyl groups, P3HMA is a stronger hydrogen donor than P2HMA¹⁴ and thus was expected to bind more strongly with PEO and to exhibit linear film growth. Figure 1B displays the opposite trend, however, with linear growth for the P2HMA/PEO rather than the P3HMA/PEO system. This trend can be explained if one suggests that gallol units are more prone to self-association compared to the catechol functionalities in P2HMA, resulting in a large polymer mass deposited at surfaces within P3HMA loops. Stronger hydrogen bonding between gallol moieties as compared to catechols has previously manifested itself in higher stability of gallol-containing supramolecular structures. ⁵² The stronger hydrogen donating capability of gallols is also supported by their higher acidity (p K_a of 9.01 and 9.45 for gallol and catechol groups, respectively).⁵³ Stronger hydrogen bonding between P3HMA units can reduce the total number of units in P3HMA chains available for binding with PEO and weaken the overall P3HMA/PEO polymer-polymer association.

The difference in mass balance between *IPPh* and PEO within hydrogen-bonded films was clearly observed in ellipsometric measurements of dry thickness during film growth. Estimates made for films thicker than four bilayers (to reduce the effect of the substrate) and using 1 g/cm³ for film density, gave molar ratios of phenolic –OH groups to ether –C–O–C– groups of PEO deposited within LbL films as 1.7±0.2 and 0.8±0.2 for P3HMA/PEO and P2HMA/PEO, respectively, indicating a significant excess of P3HMA.

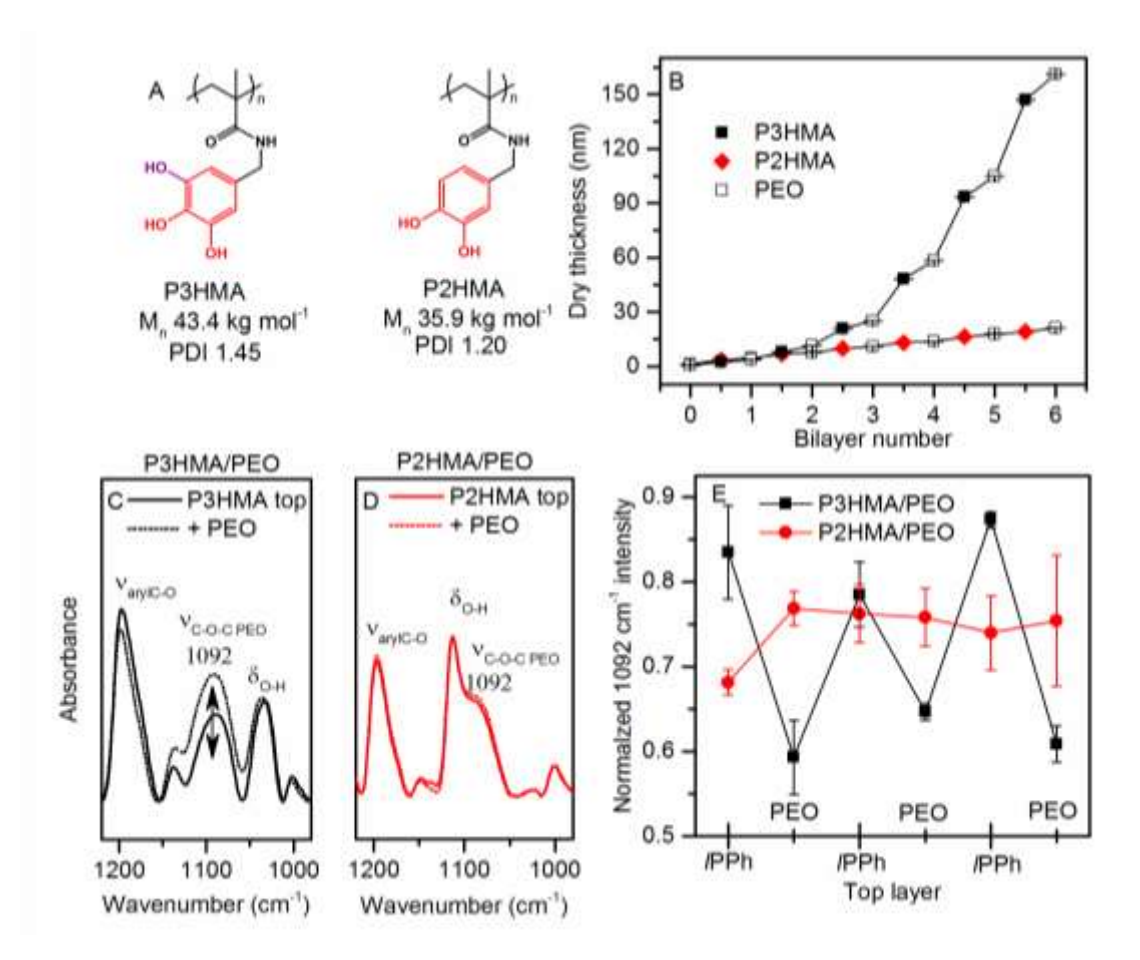


Fig. 1. Chemical structures and molecular characteristics of *IPPhs* (A); the dry thickness of *IPPh/PEO* films monitored by ellipsometry during film deposition (B); and changes in FTIR spectra of 6.5-bilayer P3HMA/PEO (C) or 50.5-bilayer P2HMA/PEO (D) films (with *IPPh* as a top layer in both cases) of matched thickness of ~200 nm in the 1250-950 cm⁻¹ region upon addition of consecutive layers (E). See Figs. S1, S2 for the entire FTIR spectra.

The composition of IPPh/PEO films was further explored using ATR-FTIR spectroscopy. Figure S1 shows the FTIR spectra of individual film components and *l*PPh/PEO films. The formation of hydrogen bonds between IPPh and PEO was observed spectroscopically by changes in a broad O-H band stretching region of lPPh, with a red shift in the band maximum from 3358 cm⁻¹ to 3355 cm⁻¹ and a significant ~50-120 cm⁻¹ narrowing from the high-wavenumber side of the band (Figure S2). Significant changes were also observed for the *IPPh/PEO* films in the 1200-1000 cm⁻¹ region, especially in the relative intensity of an ~1190 cm⁻¹ band associated with aryl -C-O stretching vibrations coupling with the skeletal vibrations of the benzene ring.⁵⁴ Changes in the vibrational intensities of covalent bonds involved in hydrogen bonding have been predicted theoretically and observed experimentally for several small organic molecules. 55,56 Figure 1E shows the variation of the integrated intensity of the 1092 cm⁻¹ C-O-C stretching vibrational band of PEO during deposition of additional layers to ~200-nm-thick P3HMA/PEO and P2HMA/PEO films. To allow for a quantitative comparison of changes in the relative amounts of PEO and IPPhs during film growth, the raw ATR-FTIR data were normalized to the intensities at 1605 cm⁻¹ and 1609 cm⁻¹, which are associated with skeletal ring vibrations of catechol and gallol pendant groups in assembled P2HMA- and P3HMAcontaining films, respectively. The changes in the intensity of the 1092 cm⁻¹ band upon deposition of additional layers were drastically different for P3HMA/PEO and P2HMA/PEO films. For exponentially growing P3HMA/PEO films, significant oscillations in intensity at 1092 cm⁻¹ occurred for successive layers, indicating the deposition of a large amount of polymer and a significant shift in the ratio of film components with each layer deposition step. In contrast, in the P2HMA/PEO system the 1092 cm⁻¹ intensity was almost unaffected by the addition of successive layers. Such behavior is expected for this linearly growing film, in which polymer adsorption was

limited to the film surface and relatively little material was added (~3 nm per bilayer) to the existing thick (~200 nm) film.

Differences in the internal structure of P3HMA/PEO and P2HMA/PEO films were then explored by neutron reflectometry, a technique we have previously applied to study the structure of electrostatically assembled and hydrogen-bonded LbL films. 18,30,57,58 To introduce contrast in neutron reflectometry measurements, fully deuterated PEO, dPEO, with M_n of 101.7 kg/mol matching the molecular weight of hydrogenated PEO of \sim 100 kg/mol, was used to create marker layers. Figure 2A depicts the design of the films used in the neutron reflectometry experiments. The films had a sandwich-like architecture featuring deuterated stacks deposited at the film

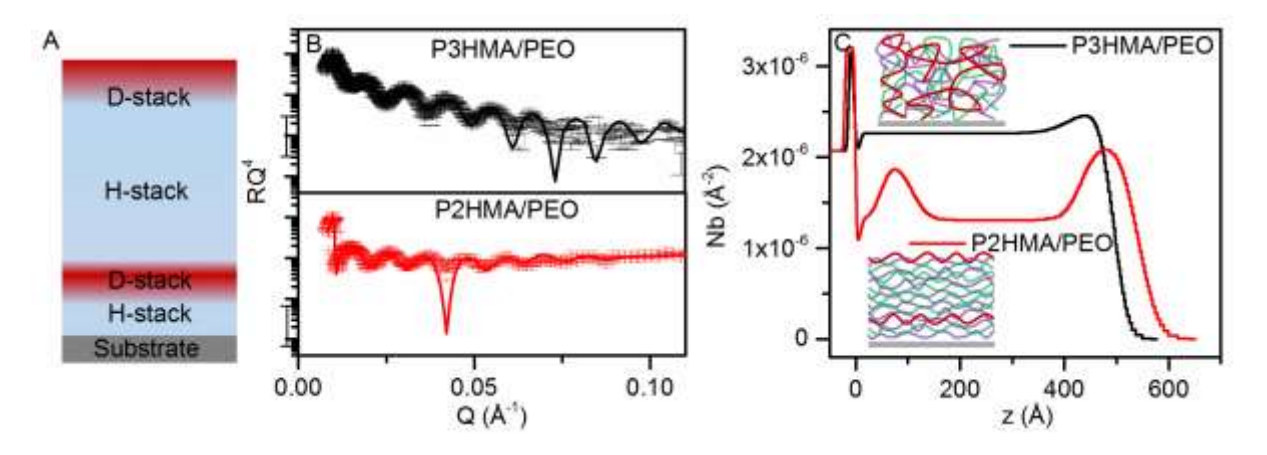


Fig. 2. Schematic of the film design, where H-stacks are built of hydrogenated PEO and *IPPh*, and D-stacks are built of deuterated PEO and *IPPh* (A); neutron reflectivity plotted as RQ^4 to highlight structural details for (P3HMA/PEO)₂/P3HMA/dPEO/P3HMA/PEO/P3HMA/dPEO and (P2HMA/PEO)₂/(P2HMA/dPEO)₂/(P2HMA/PEO)₇/(P2HMA/dPEO)₂ films (B), and the fitted neutron scattering density profiles of those films (C).

substrate and surface with a hydrogenated stack in the middle. The dry thicknesses of the stacks were measured with ellipsometry during film construction (see Tables S1, S2) and used for initial

construction of the models used to fit the neutron reflectivity data. Note that while only one dPEO layer was needed to provide scattering contrast in the P3HMA/PEO film, two bilayers were needed to accumulate enough material for P2HMA/PEO, due to the small incremental mass increase for each layer deposited. Figures 2B&C show the neutron reflectivity data and fitted neutron scattering length density (SLD) profiles for linear and exponential films. The scattering length density (SLD, Nb), the thickness of hydrogenated and deuterated stacks d, and internal roughness σ_{int} were found by fitting the reflectivity data and are shown in Tables S3 and S4 for P3HMA/PEO and P2HMA/PEO films, respectively. For the linear P2HMA/PEO film, distinct regions of higher and lower SLD were observed, associated with the deuterated and hydrogenated stacks of the deposited polymers. The boundaries between the H- and D-stacks were diffuse, with interfacial widths of 5.8 nm and 6.2 nm for the substrate- and surface-deposited deuterated blocks. In contrast, the P3HMA/PEO exponential film was highly intermixed with nearly all differences in SLD between hydrogenated and deuterated layers smeared out by molecular diffusion. Marker dPEO permeated the entire ~50-nm thickness of the P3HMA/PEO film within 5 min, while for the P2HMA/PEO film, dPEO only diffused to a depth of half the interfacial roughness of the deuterated stack within the hydrogenated matrix. The diffusion coefficients of dPEO were therefore estimated as $\sim 10^{-14}$ and ~10⁻¹⁶ cm²/s for P3HMA/PEO and P2HMA/PEO, respectively. For the P3HMA/PEO film, the estimated diffusion coefficient of ~10⁻¹⁴ cm²/s represents a lower bound and is of the same order of magnitude as the diffusion coefficients of polyelectrolytes reported for highly intermixed nonlinearly growing electrostatically assembled LbL films. 18

Figure 3 shows clear differences in the surface morphology and roughness of P3HMA/PEO and P2HMA/PEO films. The AFM root-mean-square roughnesses of these films were 5.8±2.5 nm and 2.9±0.7 nm, respectively, indicating a smoother surface on the P2HMA/PEO film. High

surface roughness was previously reported for electrostatically assembled exponential films and explained by microphase separation at the film surface, enhanced by salt-induced disruption of polymer-polymer pairing.⁵⁹

We next address how the different morphology and internal structure of IPPh/PEO films affect film functionality, *i.e.* its antioxidant activity. Confining IPPh moieties within assembled films can influence their antioxidant performance. Film swelling and the strength of polymer-polymer pairing are both expected to influence the availability of assembled IPPh units for interaction with radical species. Prior to the antioxidant studies, the stability of the films was examined. Figure S3 shows that IPPh/PEO films dissolved only when pH was raised significantly higher than the pK_a of the polyphenol moieties (9.01 and 9.45 for catechol and gallol groups)⁵³, causing

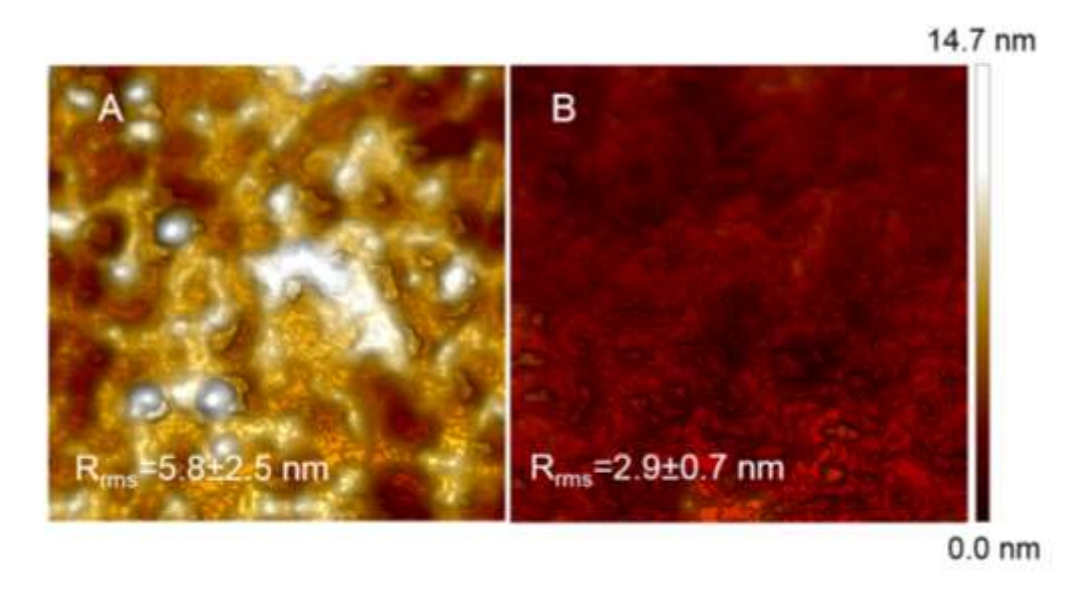


Fig. 3. AFM topography image of a 6.5-bilayer P3HMA/PEO film (A) and a 50.5-bilayer P2HMA/PEO film (B) of a matched thickness of \sim 200 nm. The scan area size is $600 \times 600 \text{ nm}^2$ and the *z*-scale shown on the right applies to both images.

ionization of hydroxyl groups in the polyphenol rings. The films were therefore stable over a wide range of pH, including the pH 6.0 at which the ABTS assay was performed.

In the ABTS assay, the number of radicals consumed over time was quantified spectroscopically by measuring the UV-Vis absorbance of ABTS^{*+} solutions at 732 nm. Quenching of colored ABTS^{*+} radicals can easily be detected visually by the bleaching of the blue-green solution. To compare the scavenging rates of ABTS^{*+} radicals by antioxidant polymers in solution to those in the film, the number of *IPPh* antioxidant monomers in solution was matched to those assembled within *IPPh/PEO* films, assuming dry polymer densities of 1 g/cm³. Figure 4 shows ABTS^{*+} scavenging is dramatically reduced relative to polymers in solution when the antioxidant polymers are assembled within films. Note that, commonly, ABTS^{*+} assays with antioxidant species in solution are performed over minutes-to-hour time scales.⁶⁰⁻⁶³ Here, we were interested

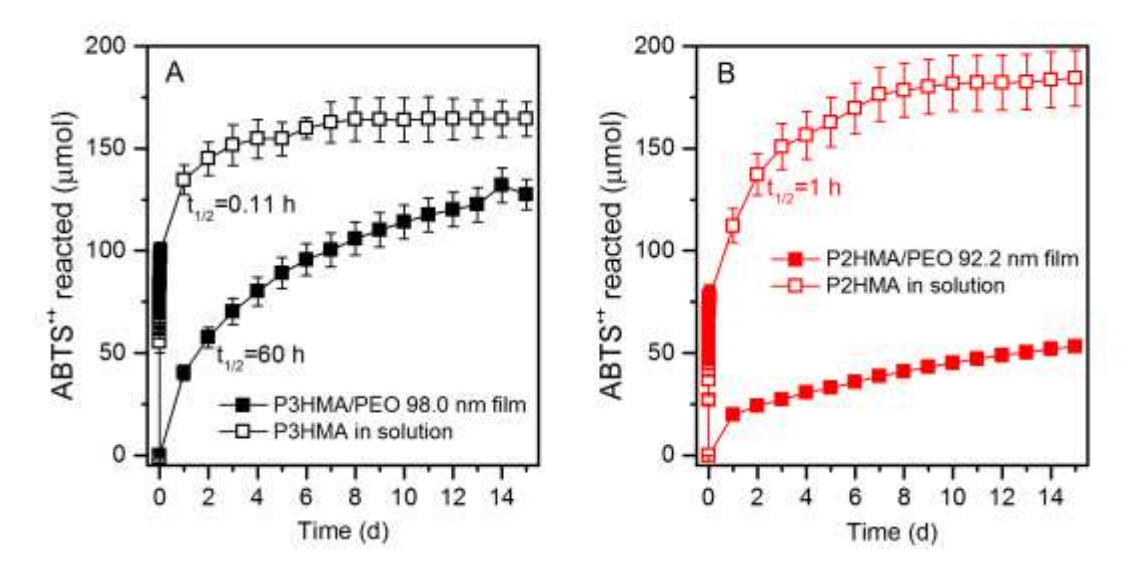


Fig. 4. Comparison of kinetics of ABTS^{*+} scavenging by matched quantities of *l*PPh antioxidant polymer dissolved in solution or assembled within a 98-nm (4.5-bilayer) P3HMA/PEO film (A) or a 92.2-nm (25.5-bilayer) P2HMA/PEO film (B). Both films had *l*PPh as a top layer.

in the long-term performance of antioxidant polymers assembled within LbL films, and therefore special care was taken to reduce the long-term degradation of stable radicals by initially purging nitrogen through the stable radical solution, followed by sealing and keeping all solutions in the dark (see Experimental sections for more details). Figure S4 shows that despite these precautions, ~20% of the initial ABTS*+ degraded in control solutions after 15 days, and that the percentage of degraded ABTS*+ was not affected by the presence of PEO in solution. All data presented in this manuscript were corrected by subtracting the degraded quantity of ABTS*+ found in the control experiment.

Figure 4 also reveals significant differences in solution *vs.* film behavior for *IPPh* with catechol and gallol functionalities. In solution, the half-life of ABTS^{*+} consumption was shorter for P3HMA than P2HMA (0.11 hour *vs* 1 hour), in agreement with the previously reported higher reactivity of low-molecular-weight polyphenols featuring more phenolic groups.⁶⁴ For *IPPhs* assembled within films, the radical scavenging rate was strongly reduced. In the case of

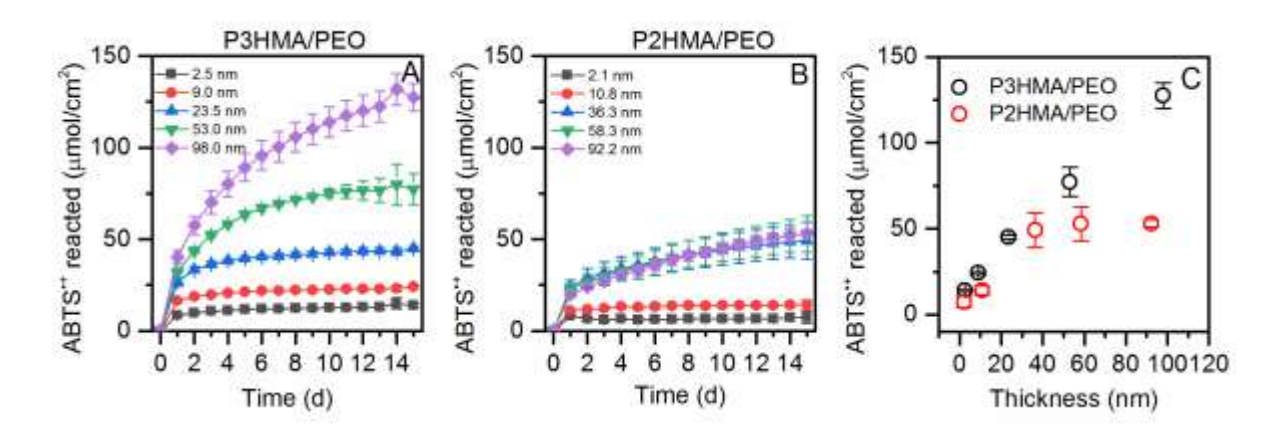
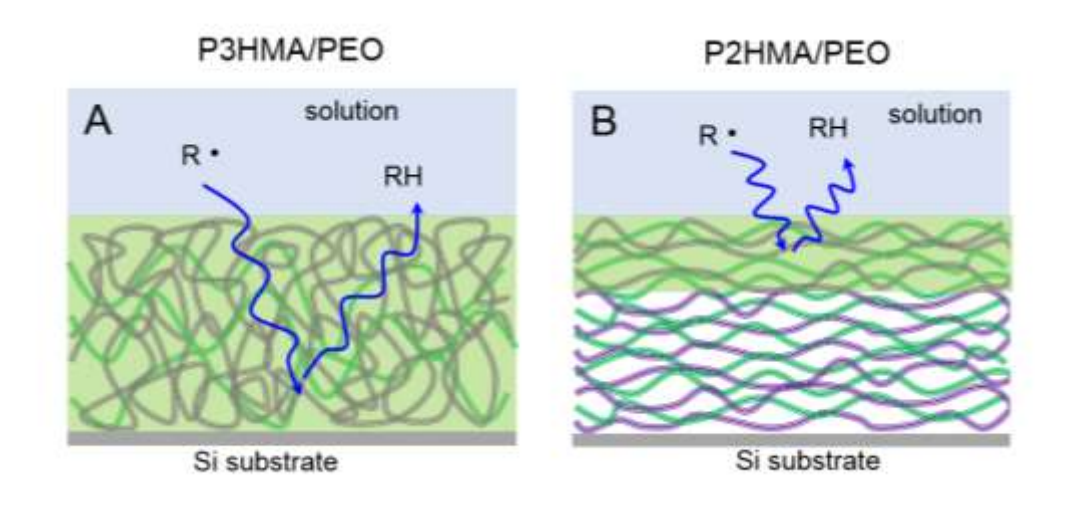


Fig. 5. Time evolution of ABTS⁺⁺ quantity reacted with P3HMA/PEO (A) and P2HMA/PEO (B) films of different thicknesses, as well as antioxidant activity of *IPPH/PEO* films assessed from the limiting values of ABTS⁺⁺ reduced after 15 days (C).

P3HMA/PEO films, the half-life of ABTS⁺⁺ consumption (~60 h) was more than two orders of magnitude longer than that for P3HMA in solution (0.11 h, Fig. 4A). For P2HMA/PEO films, the reaction rate decreased so much that half-conversion of ABTS⁺⁺ was not achieved for a 92.2-nm film even after 15 days, reaching only 30% of the polymer activity in solution (Fig. 4B). These results suggest that the impact of diffusional constraints to penetration of ABTS⁺⁺ into P2HMA/PEO films was more significant than that into P3HMA/PEO films.

To further assess differences in the radical scavenging capability of *IPPh/PEO* films, we designed experiments involving films of different thicknesses. Figure 5A-C shows that the kinetic profiles of ABTS^{*+} reduction vary differently with thickness for P3HMA/PEO and P2HMA/PEO films. While the amount of consumed ABTS^{*+} increased linearly with film thickness for P3HMA/PEO films, it saturated for films thicker than ~35 nm for P2HMA/PEO. Figure 5C compares the limiting amounts of ABTS^{*+} reacted after 15 days. Together, these data suggest a



Scheme 1. Schematic representation of ABTS^{*+} radical penetration into the bulk of the exponential P3HMA/PEO film (A), and the linear P2HMA/PEO film (B). The green area depicts the antioxidant active region.

differing availability of assembled *IPPhs* for radical scavenging. In the case of P3HMA/PEO, the entire thickness of the films reacts with ABTS^{*+}, while only the top layers of the P2HMA/PEO films were available for reaction. The thickness of P2HMA/PEO contributing to radical scavenging can be estimated from Fig. 5B as 30-35 nm. Differences in the penetration of ABTS^{*+} into *IPPh/PEO* films are illustrated in Scheme 1.

Spectroscopic ellipsometry data on *IPPh/PEO* film swelling at pH 6, *i.e.* under the same conditions used in the ABTS assay, provide additional insight into the structural determinants of free radical penetration. The data in Fig. 6A show that while P3HMA/PEO films took up ~30% water (assuming a polymer density of 1 g/cm³), P2HMA/PEO films were practically un-swollen.

The effect of uptake of water on film mechanical properties was explored using nanoindentation. These studies were performed on *IPPh/PEO* films whose thickness exceeded 0.5 µm, with tip penetration limited to 60 nm to eliminate the effect of silicon substrate. Figure 6B

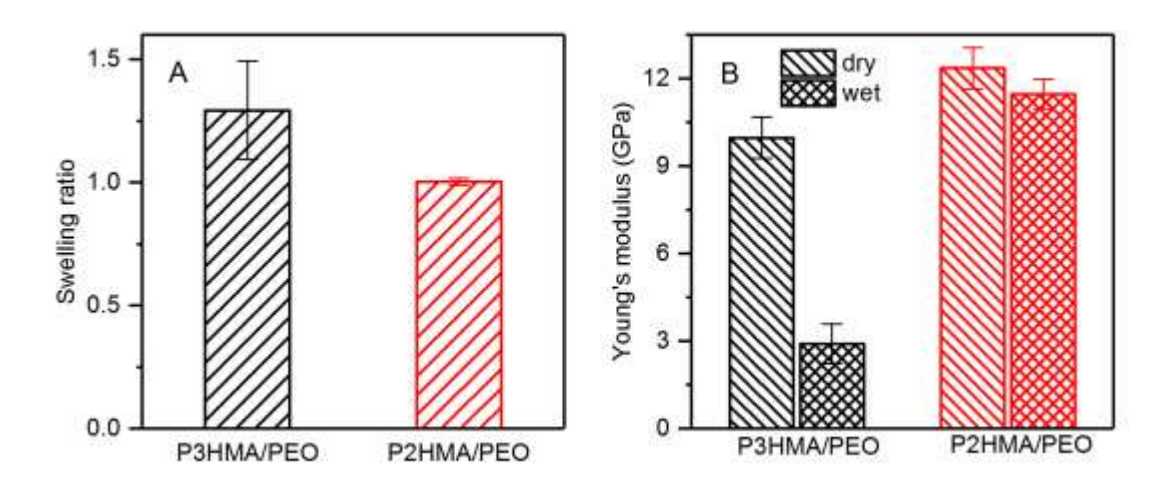


Fig. 6. The swelling ratios of a 4.5-bilayer, 98-nm P3HMA/PEO film and a 25.5-bilayer, 92.2-nm P2HMA/PEO film as measured *by in situ* ellipsometry (A) and Young's moduli of 0.6-μm-thick *l*PPh/PEO films dry and wet state (B).

shows that the Young's moduli for dry /PPh/PEO films were in the 9 to 12 GPa range. However, P3HMA/PEO and P2HMA/PEO films responded very differently upon exposure to water. While the P3HMA/PEO system underwent substantial plasticization, the Young's modulus did not significantly change for the P2HMA/PEO films. The threefold solvent-induced decrease in the Young's modulus of P3HMA/PEO films is smaller than values reported for ionically associated polyelectrolyte multilayers, ^{48,65} probably due to the low propensity of assembled /PPh chains to hydrate upon exposure to water. In spite of the insolubility of P3HMA in water, loose association between P3HMA and PEO allowed for significant water uptake within the film. This higher degree of swelling contributes to the higher antiradical activity of P3HMA/PEO films by providing a larger free volume, easing the penetration of radicals into the bulk of the film. In contrast, tighter interlayer binding within P2HMA/PEO films suppressed water uptake, leading to limited penetration of ABTS*+.

Reaction of ABTS*+ with phenolic compounds, whose redox potentials are typically lower than that of ABTS*+ (~0.7 V), has been suggested to occur predominantly via a single electron transfer (SET) mechanism.^{60,66} In the case of catechol and gallol functionalities, several reaction products have been proposed, with quinones most often formed from catechols, and oxidative crosslinking proposed as a typical reaction path.⁶⁷ A question then arises of how reaction with ABTS*+ alters the properties of the assembled films. To determine if crosslinking takes place in these LbL films, the stability of films in a competitive hydrogen-bonding solvent was assessed for pristine as-deposited films and for films exposed to ABTS*+. Figure 7A illustrates the effect of ABTS*+ on film stability. It has been observed that /PPh/PEO films dissociate to individual polymer components when the concentration of DMF – a stronger hydrogen bond acceptor than PEO^{68,69} – is above 20-30 vol %. A hydrogen-bond-accepting solvent, such as DMF or DMSO,

was previously reported to competitively bind with polymers containing hydrogen-bond-donating units, such as carboxylic groups in polyacids, resulting in a weakening in binding or a dissociation of hydrogen-polymer complexes^{70,71} or hydrogen-bonded LbL films.^{72,73} In this work, DMF formed hydrogen bonds with polyphenol groups of assembled *IPPh*, and dissolved P3HMA/PEO and P2HMA/PEO films when DMF content exceeded 20 and 30 vol %, respectively. The higher stability of P2HMA/PEO assemblies in DMF solutions is consistent with a larger number of hydrogen bonds with PEO per P2HMA moiety in this linearly growing system. Remarkably, exposure to ABTS⁺⁺ resulted in a drastic increase in the stability of the films, which did not dissolve in DMF up to 70 vol % (Fig. 7A), but delaminated from the surface at higher DMF concentrations.

To identify chemical changes in the *IPPh/PEO* film triggered by the reaction of *IPPh* with ABTS⁺, FTIR measurements were performed before and after long-term exposure to solutions of the radical species. FTIR spectra shown in Figure 7B indicate a significant increase in absorbance

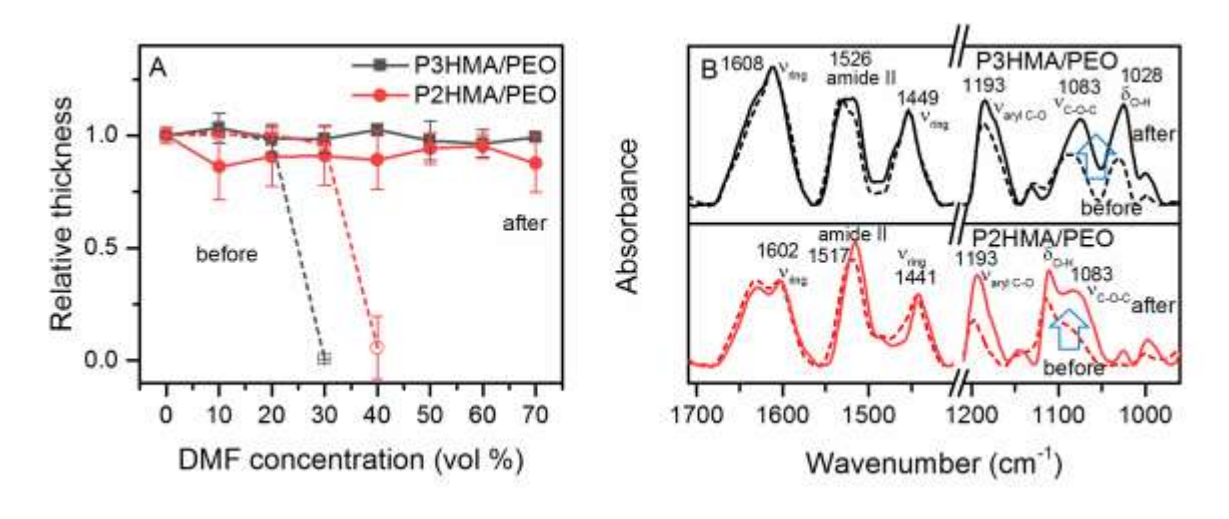


Fig. 7. Stability of 6.5-bilayer P3HMA/PEO and 50.5-bilayer P2HMA/PEO films with a matched thickness of ~200 nm in the DMF/water mixed solution before (dotted line) and after (solid line) exposure to 0.075 mM solutions of ABTS*+ for 15 days (A), as well ATR-FTIR spectra of the films before and after a 5-day assay (B).

of *IPPh/PEO* films in the 1000-1200 cm⁻¹ region after exposure to ABTS^{*+} solutions. Increased intensities of a band at 1193 cm⁻¹, which is associated with aryl -C–O stretching vibrations coupled with skeletal vibrations of the benzene ring, as well as of a band at 1083 cm⁻¹, which is assigned to -C–O–C- stretching vibrations, ^{54,74} are both consistent with the formation of ether bonds as a result of radical-induced coupling of polyphenol rings (Schemes S1 and S2).

In conclusion, we have found fundamental differences in LbL assembly of synthetic linear polyphenols with gallol- and catechol pendant groups and demonstrated the dramatic effect of these differences on film functionality. Specifically, the film growth mode, structure, and antioxidant activity were all strongly influenced by the chemical structure of the polyphenol rings. Overall, antioxidant performance is determined by the total number of functional groups available in the film to consume radicals. This, in turn, depends on the presence of sufficient free volume in the film to allow penetration of radicals and on the local density of functional groups. In this work, we found that a propensity of gallol groups to self-association resulted in a twofold effect of P3HMA polymer on film performance. First, this character resulted in exponential film growth, in which polymer chains were strongly intermixed. Weak intermolecular binding within those films led to film swelling and engagement of polyphenol units throughout the entire film thickness in radical scavenging reactions. Second, introduction of this polymer within the films dramatically changed film composition, resulting in increased local density of polyphenol functional groups. In contrast, a catechol-based P2HMA polyphenol formed linearly grown films that restricted the penetration of radical species, thus confining radical scavenging to the surface layers of the films. This work demonstrates how the chemical structure of polyphenol units can control their hydrogen bonding within LbL films and can program film structure, swelling, and availability of polyphenol units for interaction with radical species.

Supporting Information

Ellipsometric thickness during film construction; fitting parameters of neutron reflectivity studies, FTIR spectra, /PPh/PEO films pH stability, ABTS*+ self-degradation data.

This material is available free of charge online at http://pubs.acs.org.

Corresponding Author

*E-mail: svetlana@tamu.edu.

Notes

The authors declare no competing financial interest.

Acknowledgment

This work was supported by the National Science Foundation under Award DMR-1610725 and DMR-1905535 (S.S.). Neutron measurements were performed at the Spallation Neutron Source at the Oak Ridge National Laboratory, managed by UT-Battelle, LLC, for the DOE under contract No. DE-AC05-00OR. We thank Qing Zhou for help with AFM measurements and Hanna Hlushko for helpful comments on the manuscript. Use of the TAMU Materials Characterization Facility is acknowledged.

References

- (1) Jamshidian, M.; Tehrany, E. A.; Imran, M.; Akhtar, M. J.; Cleymand, F.; Desobry, S. Structural, mechanical and barrier properties of active PLA-antioxidant films. *J. Food Eng.* **2012**, *110*, 380-389.
- (2) Hager, A.-S.; Vallons, K. J. R.; Arendt, E. K. Influence of Gallic Acid and Tannic Acid on the Mechanical and Barrier Properties of Wheat Gluten Films. *J. Agric. Food Chem.* **2012**, *60*, 6157-6163.
- (3) Pant, A. F.; Sängerlaub, S.; Müller, K. Gallic Acid as an Oxygen Scavenger in Bio-Based Multilayer Packaging Films. *Materials* **2017**, *10*, 489.
- (4) Iñiguez-Franco, F.; Soto-Valdez, H.; Peralta, E.; Ayala-Zavala, J. F.; Auras, R.; Gámez-Meza, N. Antioxidant Activity and Diffusion of Catechin and Epicatechin from Antioxidant Active Films Made of Poly(l-lactic acid). *J. Agric. Food Chem.* **2012**, *60*, 6515-6523.
- (5) Sun, X.; Wang, Z.; Kadouh, H.; Zhou, K. The antimicrobial, mechanical, physical and structural properties of chitosan–gallic acid films. *LWT Food Sci. Technol.* **2014**, *57*, 83-89.
- (6) Luzi, F.; Fortunati, E.; Giovanale, G.; Mazzaglia, A.; Torre, L.; Balestra, G. M. Cellulose nanocrystals from Actinidia deliciosa pruning residues combined with carvacrol in PVA_CH films with antioxidant/antimicrobial properties for packaging applications. *Int. J. of Biol. Macromol.* **2017**, *104*, 43-55.
- (7) Nerín, C.; Tovar, L.; Salafranca, J. Behaviour of a new antioxidant active film versus oxidizable model compounds. *J. Food Eng.* **2008**, *84*, 313-320.
- (8) Zhu, J.; Wu, H.; Sun, Q. Preparation of crosslinked active bilayer film based on chitosan and alginate for regulating ascorbate-glutathione cycle of postharvest cherry tomato (Lycopersicon esculentum). *Int. J. Biol. Macromol.* **2019**, *130*, 584-594.
- (9) Gemili, S.; Yemenicioğlu, A.; Altınkaya, S. A. Development of antioxidant food packaging materials with controlled release properties. *J. Food Eng.* **2010**, *96*, 325-332.
- (10) Liu, J.; Liu, S.; Chen, Y.; Zhang, L.; Kan, J.; Jin, C. Physical, mechanical and antioxidant properties of chitosan films grafted with different hydroxybenzoic acids. *Food Hydrocoll.* **2017**, *71*, 176-186.
- (11) Hu, X.; Liu, S.; Zhou, G.; Huang, Y.; Xie, Z.; Jing, X. Electrospinning of polymeric nanofibers for drug delivery applications. *J. Controll. Release* **2014**, *185*, 12-21.

- (12) Oh, D. X.; Kim, S.; Lee, D.; Hwang, D. S. Tunicate-mimetic nanofibrous hydrogel adhesive with improved wet adhesion. *Acta Biomater.* **2015**, *20*, 104-112.
- (13) Hu, Q.; Wang, T.; Zhou, M.; Xue, J.; Luo, Y. In Vitro Antioxidant-Activity Evaluation of Gallic-Acid-Grafted Chitosan Conjugate Synthesized by Free-Radical-Induced Grafting Method. *J. Agric. Food Chem.* **2016**, *64*, 5893-5900.
- (14) Hlushko, R.; Hlushko, H.; Sukhishvili, S. A. A family of linear phenolic polymers with controlled hydrophobicity, adsorption and antioxidant properties. *Polym. Chem.* **2018**, *9*, 506-516.
- (15) Zhan, K.; Ejima, H.; Yoshie, N. Antioxidant and Adsorption Properties of Bioinspired Phenolic Polymers: A Comparative Study of Catechol and Gallol. *ACS Sustain. Chem. Eng.* **2016**, *4*, 3857-3863.
- (16) Decher, G.; Hong, J. D.; Schmitt, J. Buildup of ultrathin multilayer films by a self-assembly process: III. Consecutively alternating adsorption of anionic and cationic polyelectrolytes on charged surfaces. *Thin Solid Films* **1992**, *210-211*, 831-835.
- (17) Decher, G. Fuzzy Nanoassemblies: Toward Layered Polymeric Multicomposites. *Science* **1997**, *277*, 1232-1237.
- (18) Selin, V.; Ankner, J. F.; Sukhishvili, S. A. Nonlinear Layer-by-Layer Films: Effects of Chain Diffusivity on Film Structure and Swelling. *Macromolecules* **2017**, *50*, 6192-6201.
- (19) Picart, C.; Mutterer, J.; Richert, L.; Luo, Y.; Prestwich, G. D.; Schaaf, P.; Voegel, J. C.; Lavalle, P. Molecular basis for the explanation of the exponential growth of polyelectrolyte multilayers. *Proc. Natl. Acad. Sci. U S A* **2002**, *99*, 12531-12535.
- (20) Liu, G.; Zou, S.; Fu, L.; Zhang, G. Roles of Chain Conformation and Interpenetration in the Growth of a Polyelectrolyte Multilayer. *J. Phys. Chem. B* **2008**, *112*, 4167-4171.
- (21) Xu, L.; Pristinski, D.; Zhuk, A.; Stoddart, C.; Ankner, J. F.; Sukhishvili, S. A. Linear versus Exponential Growth of Weak Polyelectrolyte Multilayers: Correlation with Polyelectrolyte Complexes. *Macromolecules* **2012**, *45*, 3892-3901.
- (22) Stockton, W. B.; Rubner, M. F. Molecular-Level Processing of Conjugated Polymers. 4. Layer-by-Layer Manipulation of Polyaniline via Hydrogen-Bonding Interactions. *Macromolecules* **1997**, *30*, 2717-2725.

- (23) Wang, L.; Wang, Z.; Zhang, X.; Shen, J.; Chi, L.; Fuchs, H. A new approach for the fabrication of an alternating multilayer film of poly(4-vinylpyridine) and poly(acrylic acid) based on hydrogen bonding. *Macromol. Rapid. Comm.* **1997**, *18*, 509-514.
- (24) Kozlovskaya, V.; Ok, S.; Sousa, A.; Libera, M.; Sukhishvili, S. A. Hydrogen-Bonded Polymer Capsules Formed by Layer-by-Layer Self-Assembly. *Macromolecules* **2003**, *36*, 8590-8592.
- (25) Fu, Y.; Bai, S.; Cui, S.; Qiu, D.; Wang, Z.; Zhang, X. Hydrogen-Bonding-Directed Layer-by-Layer Multilayer Assembly: Reconformation Yielding Microporous Films. *Macromolecules* **2002**, *35*, 9451-9458.
- (26) Sukhishvili, S. A.; Granick, S. Layered, Erasable, Ultrathin Polymer Films. *J. Am. Chem. Soc.* **2000**, *122*, 9550-9551.
- (27) Sukhishvili, S. A.; Granick, S. Layered, Erasable Polymer Multilayers Formed by Hydrogen-Bonded Sequential Self-Assembly. *Macromolecules* **2002**, *35*, 301-310.
- (28) Wang, X.; Liu, F.; Zheng, X.; Sun, J. Water-Enabled Self-Healing of Polyelectrolyte Multilayer Coatings. *Angew. Chem.* **2011**, *50*, 11378-11381.
- (29) Cheng, M.; Shi, F.; Li, J.; Lin, Z.; Jiang, C.; Xiao, M.; Zhang, L.; Yang, W.; Nishi, T. Macroscopic Supramolecular Assembly of Rigid Building Blocks Through a Flexible Spacing Coating. *Adv. Mater.* **2014**, *26*, 3009-3013.
- (30) Selin, V.; Ankner, J. F.; Sukhishvili, S. A. Ionically Paired Layer-by-Layer Hydrogels: Water and Polyelectrolyte Uptake Controlled by Deposition Time. *Gels* **2018**, *4*, 7.
- (31) Kharlampieva, E.; Sukhishvili, S. A. Release of a Dye from Hydrogen-Bonded and Electrostatically Assembled Polymer Films Triggered by Adsorption of a Polyelectrolyte. *Langmuir* **2004**, *20*, 9677-9685.
- (32) Pavlukhina, S.; Zhuk, I.; Mentbayeva, A.; Rautenberg, E.; Chang, W.; Yu, X.; van de Belt-Gritter, B.; Busscher, H. J.; van der Mei, H. C.; Sukhishvili, S. A. Small-molecule-hosting nanocomposite films with multiple bacteria-triggered responses. *NPG Asia Mater.* **2014**, *6*, 121.
- (33) Mentbayeva, A.; Ospanova, A.; Tashmuhambetova, Z.; Sokolova, V.; Sukhishvili, S. Polymer–Metal Complexes in Polyelectrolyte Multilayer Films as Catalysts for Oxidation of Toluene. *Langmuir* **2012**, *28*, 11948-11955.
- (34) Erel-Unal, I.; Sukhishvili, S. A. Hydrogen-Bonded Multilayers of a Neutral Polymer and a Polyphenol. *Macromolecules* **2008**, *41*, 3962-3970.

- (35) Kozlovskaya, V.; Shamaev, A.; Sukhishvili, S. A. Tuning swelling pH and permeability of hydrogel multilayer capsules. *Soft Matter* **2008**, *4*, 1499-1507.
- (36) Ninan, N.; Forget, A.; Shastri, V. P.; Voelcker, N. H.; Blencowe, A. Antibacterial and Anti-Inflammatory pH-Responsive Tannic Acid-Carboxylated Agarose Composite Hydrogels for Wound Healing. *ACS Appl. Mater. Interfaces* **2016**, *8*, 28511-28521.
- (37) Kozlovskaya, V.; Xue, B.; Lei, W.; Padgett, L. E.; Tse, H. M.; Kharlampieva, E. Hydrogen-Bonded Multilayers of Tannic Acid as Mediators of T Cell Immunity. *Adv. Healthc.* **2015**, *4*, 686-694.
- (38) Zhao, Y.-N.; Gu, J.; Jia, S.; Guan, Y.; Zhang, Y. Zero-order release of polyphenolic drugs from dynamic, hydrogen-bonded LBL films. *Soft Matter* **2016**, *12*, 1085-1092.
- (39) Madrigal-Carballo, S.; Lim, S.; Rodriguez, G.; Vila, A. O.; Krueger, C. G.; Gunasekaran, S.; Reed, J. D. Biopolymer coating of soybean lecithin liposomes via layer-by-layer self-assembly as novel delivery system for ellagic acid. *J. Funct. Foods* **2010**, *2*, 99-106.
- (40) Shutava, T. G.; Balkundi, S. S.; Lvov, Y. M. (–)-Epigallocatechin gallate/gelatin layer-by-layer assembled films and microcapsules. *J. Colloid Interface Sci.* **2009**, *330*, 276-283.
- (41) Hlushko, H.; Cubides, Y.; Hlushko, R.; Kelly, T. M.; Castaneda, H.; Sukhishvili, S. A. Hydrophobic Antioxidant Polymers for Corrosion Protection of an Aluminum Alloy. *ACS Sustain. Chem. Eng* **2018**, *6*, 14302-14313.
- (42) Rahim, M. A.; Kristufek, S. L.; Pan, S.; Richardson, J. J.; Caruso, F. Phenolic Building Blocks for the Assembly of Functional Materials. *Angew. Chem.* **2019**, *58*, 1904-1927.
- (43) Ryu, J. H.; Messersmith, P. B.; Lee, H. Polydopamine Surface Chemistry: A Decade of Discovery. *ACS Appl Mater. Interfaces* **2018**, *10*, 7523-7540.
- (44) Dubas, S. T.; Schlenoff, J. B. Factors controlling the growth of polyelectrolyte multilayers. *Macromolecules* **1999**, *32*, 8153-8160.
- (45) Kozlovskaya, V.; Yakovlev, S.; Libera, M.; Sukhishvili, S. A. Surface Priming and the Self-Assembly of Hydrogen-Bonded Multilayer Capsules and Films. *Macromolecules* **2005**, *38*, 4828-4836.
- (46) Woollam, J. A.; Johs, B. D.; Herzinger, C. M.; Hilfiker, J. N.; Synowicki, R. A.; Bungay, C. L.: Overview of variable-angle spectroscopic ellipsometry (VASE): I. Basic theory and typical applications; SPIE, **1999**; 10294.

- (47) Oliver, W. C.; Pharr, G. M. Measurement of hardness and elastic modulus by instrumented indentation: Advances in understanding and refinements to methodology. *J. Mater. Res.* **2011**, *19*, 3-20.
- (48) Nolte, A. J.; Rubner, M. F.; Cohen, R. E. Determining the Young's Modulus of Polyelectrolyte Multilayer Films via Stress-Induced Mechanical Buckling Instabilities. *Macromolecules* **2005**, *38*, 5367-5370.
- (49) Cai, H.; Liu, X.; Zou, J.; Xiao, J.; Yuan, B.; Li, F.; Cheng, Q. Multi-wavelength spectrophotometric determination of hydrogen peroxide in water with peroxidase-catalyzed oxidation of ABTS. *Chemosphere* **2018**, *193*, 833-839.
- (50) Garza, J. M.; Schaaf, P.; Muller, S.; Ball, V.; Stoltz, J.-F.; Voegel, J.-C.; Lavalle, P. Multicompartment Films Made of Alternate Polyelectrolyte Multilayers of Exponential and Linear Growth. *Langmuir* **2004**, *20*, 7298-7302.
- (51) Bieker, P.; Schönhoff, M. Linear and Exponential Growth Regimes of Multilayers of Weak Polyelectrolytes in Dependence on pH. *Macromolecules* **2010**, *43*, 5052-5059.
- (52) Cohen, Y.; Evan-Salem, T.; Avram, L. Hydrogen-Bonded Hexameric Capsules of Resorcin[4]arene, Pyrogallol[4]arene and Octahydroxypyridine[4]arene are Abundant Structures in Organic Solvents: A View from Diffusion NMR. *Supramol. Chem.* **2008**, *20*, 71-79.
- (53) Serjeant, E. P.; Dempsey, B.; *Ionisation constants of organic acids in aqueous solution*; Pergamon Press: Oxford; New York, **1979**.
- (54) Ricci, A.; Olejar, K. J.; Parpinello, G. P.; Kilmartin, P. A.; Versari, A. Application of Fourier Transform Infrared (FTIR) Spectroscopy in the Characterization of Tannins. *Appl. Spectrosc. Rev.* **2015**, *50*, 407-442.
- (55) Mitsuzuka, A.; Fujii, A.; Ebata, T.; Mikami, N. Infrared Spectroscopy of Intramolecular Hydrogen-Bonded OH Stretching Vibrations in Jet-Cooled Methyl Salicylate and Its Clusters. *J. Phys. Chem. A* **1998**, *102*, 9779-9784.
- (56) Dimitrova, Y. Theoretical study of the changes in the vibrational characteristics arising from the hydrogen bonding between Vitamin C (l-ascorbic acid) and H2O. *Spectrochim. Acta A* **2006**, *63*, 427-437.
- (57) Xu, L.; Selin, V.; Zhuk, A.; Ankner, J. F.; Sukhishvili, S. A. Molecular Weight Dependence of Polymer Chain Mobility within Multilayer Films. *ACS Macro Letters* **2013**, *2*, 865-868.

- (58) Selin, V.; Ankner, J. F.; Sukhishvili, S. A. Diffusional Response of Layer-by-Layer Assembled Polyelectrolyte Chains to Salt Annealing. *Macromolecules* **2015**, *48*, 3983-3990.
- (59) McAloney, R. A.; Dudnik, V.; Goh, M. C. Kinetics of Salt-Induced Annealing of a Polyelectrolyte Multilayer Film Morphology. *Langmuir* **2003**, *19*, 3947-3952.
- (60) Prior, R. L.; Wu, X.; Schaich, K. Standardized Methods for the Determination of Antioxidant Capacity and Phenolics in Foods and Dietary Supplements. *J. Agric. Food Chem.* **2005**, *53*, 4290-4302.
- (61) Hotta, H.; Nagano, S.; Ueda, M.; Tsujino, Y.; Koyama, J.; Osakai, T. Higher radical scavenging activities of polyphenolic antioxidants can be ascribed to chemical reactions following their oxidation. *Biochim. Biophys. Acta* **2002**, *1572*, 123-132.
- (62) Koleva, I. I.; Niederländer, H. A. G.; van Beek, T. A. Application of ABTS Radical Cation for Selective On-Line Detection of Radical Scavengers in HPLC Eluates. *Anal. Chem.* **2001**, *73*, 3373-3381.
- (63) Tian, X.; Schaich, K. M. Effects of Molecular Structure on Kinetics and Dynamics of the Trolox Equivalent Antioxidant Capacity Assay with ABTS+•. *J. Agric. Food Chem.* **2013**, *61*, 5511-5519.
- (64) Siquet, C.; Paiva-Martins, F.; Lima, J. L. F. C.; Reis, S.; Borges, F. Antioxidant profile of dihydroxy- and trihydroxyphenolic acids-A structure–activity relationship study. *Free Radic. Res.* **2006**, *40*, 433-442.
- (65) Lehaf, A. M.; Hariri, H. H.; Schlenoff, J. B. Homogeneity, Modulus, and Viscoelasticity of Polyelectrolyte Multilayers by Nanoindentation: Refining the Buildup Mechanism. *Langmuir* **2012**, *28*, 6348-6355.
- (66) Huang, D.; Ou, B.; Prior, R. L. The Chemistry behind Antioxidant Capacity Assays. *J. Agric. Food Chem.* **2005**, *53*, 1841-1856.
- (67) Kandaswami, C.; Vaidyanathan, C. S. Oxidation of catechol in plants. *Biochem. J.* **1972**, *128*, 30P-31P.
- (68) Huang, Z.; Yu, L.; Dai, Y.; Wang, H. Hydrogen bonding interactions between N,N-dimethylformamide and cysteine: DFT studies of structures, properties, and topologies. J. *Struct. Chem.* **2011**, *22*, 57-65.
- (69) Zhang, C.; Ren, Z.; Liu, L.; Yin, Z. Modelling hydrogen bonds in NN-dimethylformamide. *Mol. Simulat.* **2013**, *39*, 875-881.

- (70) Khutoryanskiy, V.; Staikos, G.: *Hydrogen-Bonded Interpolymer Complexes*; World Scientific Publishing Co. Pte. Ltd., **2009**.
- (71) Wang, Y. H.; He, J.; Aktas, S.; Sukhishvili, S. A.; Kalyon, D. M. Rheological behavior and self-healing of hydrogen-bonded complexes of a triblock Pluronic((R)) copolymer with a weak polyacid. *J. Rheol.* **2017**, *61*, 1103-1119.
- (72) Ma, S.; Yuan, Q.; Zhang, X.; Yang, S.; Xu, J. Solvent effect on hydrogen-bonded thin film of poly(vinylpyrrolidone) and poly(acrylic acid) prepared by layer-by-layer assembly. *Colloid. Surface A* **2015**, *471*, 11-18.
- (73) Selin, V.; Aliakseyeu, A.; Ankner, J. F.; Sukhishvili, S. A. Effect of a Competitive Solvent on Binding Enthalpy and Chain Intermixing in Hydrogen-Bonded Layer-by-Layer Films. *Macromolecules* **2019**.
- (74) Jennings, K. R. Spectrometric identification of organic compounds (Fifth Edition). R. M. Silverstein, G. C. Bassler and T. C. Morrill, Wiley, New York, **1991**.

For Table of Contents Only

Layer-by-Layer Hydrogen-Bonded Antioxidant Films of Linear Synthetic Polyphenols

Raman Hlushko¹, John F. Ankner², and Svetlana Sukhishvili¹*

¹Department of Materials Science and Engineering, Texas A&M University

College Station, Texas 77843, USA

²Spallation Neutron Source, Oak Ridge National Laboratory, Oak Ridge, Tennessee 37831, USA

